Prestack migration using the linearly transformed wave equation method

Zhiming Li

ABSTRACT

A profile migration method, using the linearly transformed wave equation (LITWEQ) method, is presented in this paper. Both synthetic and field-data examples show satisfactory results of applying the LITWEQ method to prestack migration.

INTRODUCTION

Although common-midpoint (CMP) stacking (Mayne, 1962) has the advantage of improving signal-to-noise ratios and reducing data sizes before migration, it has the disadvantage of averaging reflectivities over certain segments of reflectors when reflectors are dipping, or when the earth is laterally inhomogeneous. This averaging of reflectivities distorts pictures of underground structures, in particular obscuring details of reflectivity changes such that analysis of seismic stratigraphy becomes difficult. Other disadvantages of CMP stacking include data aliasing (of dipping reflections) in CMP gathers, and high computer I/O expense for sorting CMP gathers. To overcome these problems, prestack migration (i.e., imaging before stacking) (Claerbout, 1976; Jacobs, 1982) and partial prestack migration (i.e., dip-moveout) (Judson et al., 1978; Hale, 1983) have been introduced in the seismic industry over the years.

As an application of the LITWEQ method (Li, 1985), LITWEQ prestack profile migration is applied to 56 shot profiles taken from the Gulf of Mexico. In these migrated profiles, some fault-plane reflections are preserved and imaged at the correct locations of the fault planes. Stacking over all the migrated profiles significantly enhances the images of the underground structure, while suppressing multiple reflections and some computational artifacts. Further applications of the LITWEQ profile migration may be in velocity analysis (inversion) and multiple-reflection imaging.

PROFILE MIGRATION USING THE LITWEQ METHOD

Forward modeling

Shot profile migration consists in matching forward modeling of a downgoing wavefield (generated by a given velocity and source model), with a backward extrapolation of upcoming reflections (recorded at the earth's surface). Both the forward modeling and the backward extrapolation can be done by the LITWEQ method (Li, SEP-41 and SEP-42).

Under the transformed coordinates (x, t_1, t_2), LITWEQ forward modeling is required only in the region enclosed by three lines: $t_1 = (t + \tau)/\sqrt{2} = t_{\max}/\sqrt{2}$, $t_1 = t_2$ and $t_1 = -t_2$, where $t_{\max}$ is the maximum record time and τ is the pseudo-depth. The computation can be further reduced to the region enclosed by $t_1 = t_{\max}/\sqrt{2}$, $t_2 = \tau_{smax}/\sqrt{2}$, $t_1 = t_2$ and $t_1 = -t_2$ (Figure 1), if the maximum pseudo-depth of the source is τ_{smax}.

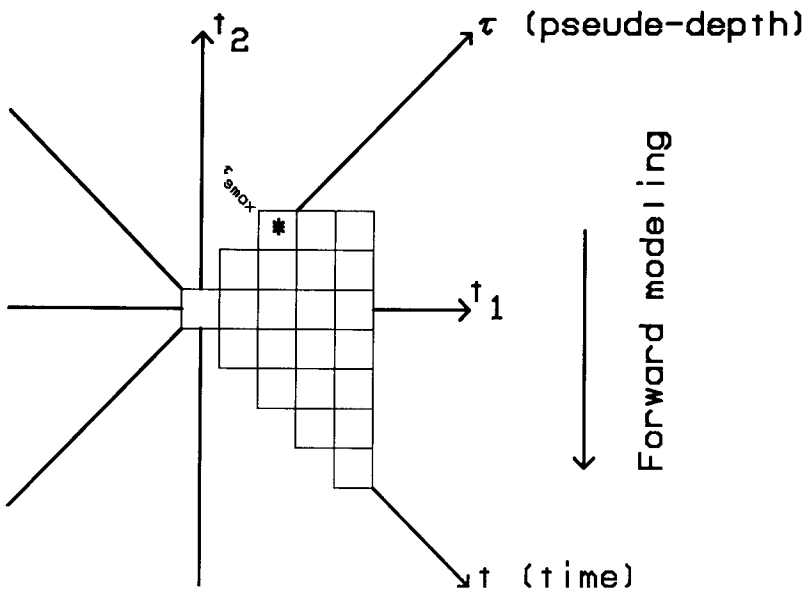

FIG. 1. Computation grids for finite-difference LITWEQ forward modeling of downgoing waves in (t_1, t_2) plane. Maximum depth of source location is at $\tau = \tau_{smax}$. The source is denoted by *. For surface source, $\tau_{smax} = 0$, computation can be reduced to those grids in the figure with $t_2 \leq 0$.

Backward extrapolation

With the wavefield $P(x, t_1{=}t/\sqrt{2}, t_2{=}{-}t/\sqrt{2})$ recorded at the earth's surface, the backward (in time) extrapolation of $P(x, t_1, t_2)$ in the LITWEQ coordinates is carried out in the region enclosed by $t_1 = t_{\max}/\sqrt{2}$, $t_2 = \tau_{smax}/\sqrt{2}$, $t_1 = t_2$ and $t_1 = -t_2$ (Figure 2).

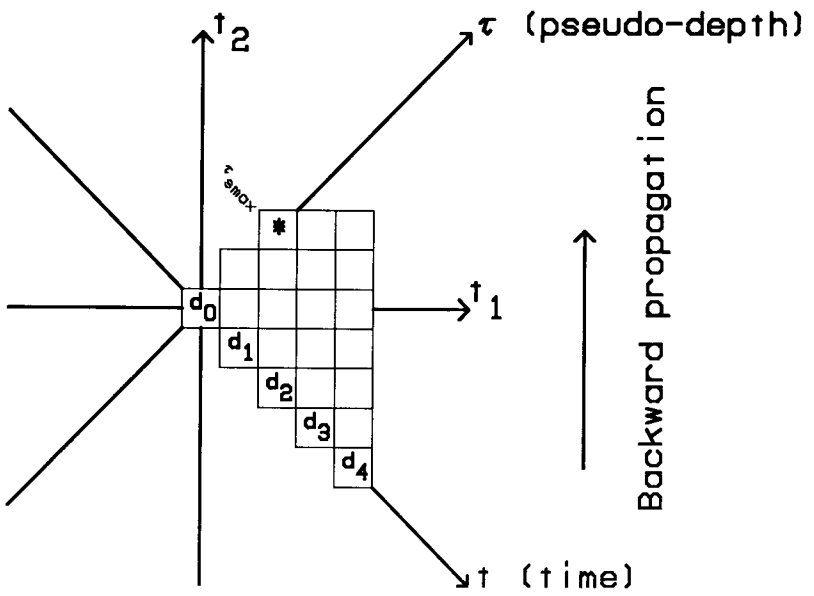

FIG. 2. Computation grids for finite-difference LITWEQ backward extrapolation of upcoming reflections in (t_1, t_2) plane. The surface data are denoted by d_i's.

Because some reflections (dipping-bed reflections) in a seismic profile may come from reflectors whose locations are outside the profile, some traces should be padded at both sides of the profile before forward modeling and backward extrapolating, especially on the near-offset side. The number of traces needed depends on both the angles of the dipping reflectors and the velocity distribution. In backward extrapolation, it is better to pad seismic traces selected from other shot profiles according to reciprocity of source and receiver than to pad traces of all zeros, to enhance resolution of imaging. However, it is likely that we need to interpolate between these padded traces unless receiver spacing is equal to an integer multiple of shot spacing.

Imaging by zero-lag cross-correlation

After the above two processes (forward modeling and backward extrapolation) are completed, a migrated profile can be obtained by correlating the two separate wavefields.

For any moment t at any underground position $(x\,,\,z)$, the reflected wavefield $B(x\,,\,z\,,\,t)$ (the result of backward extrapolation) must be equal to the incident wavefield $F(x\,,\,z\,,\,t)$ (the result of forward modeling) times the reflectivity $C(x\,,\,z)$, i.e.,

$$B(x\,,\,z\,,\,t) \;=\; F(x\,,\,z\,,\,t)\;C(x\,,\,z)\;. \tag{1}$$

Since reflectivity is time-independent (physical properties of the earth do not change during a survey), $C(x\,,\,z)$ can be estimated by least-squares principles, giving

$$C_0(x\,,\,z) \;=\; \frac{1}{NT}\sum_{it=1}^{NT}\frac{B(x\,,\,z\,,\,it)}{F(x\,,\,z\,,\,it)}\;, \tag{2}$$

where NT is the number of the time samples per trace. This summation over time axis in estimating reflectivity enhances coherent images of primary reflections, while suppressing incoherent noises.

Estimation of reflectivity by equation (2) is usually unstable because small values of $F(x\,,\,z\,,\,t)$ cause overflow problems in computation. Three other approximate, but feasible, estimations of $C(x\,,\,z)$ from time-dependent data $B(x\,,\,z\,,\,t)$ and $F(x\,,\,z\,,\,t)$ are summarized as follows, analogously to Jacobs' Fourier domain estimations (Jacobs, 1982):

$$C_1(x\,,\,z) \;=\; \frac{1}{NT}\sum_{it=1}^{NT} W(x\,,\,z\,,\,t)\;B(x\,,\,z\,,\,t)\;F(x\,,\,z\,,\,t)\;, \tag{3}$$

$$C_2(x\,,\,z) \;=\; \frac{1}{NT}\sum_{it=1}^{NT} W(x\,,\,z\,,\,t)\;B(x\,,\,z\,,\,t)\;\mathbf{sign}[F(x\,,\,z\,,\,t)]\;,\;\text{and} \tag{4}$$

$$C_2(x\,,\,z) \;=\; \frac{1}{NT}\sum_{it=1}^{NT} W(x\,,\,z\,,\,t)\;\frac{B(x\,,\,z\,,\,t)\;F(x\,,\,z\,,\,t)}{|\,F(x\,,\,z\,,\,t)\,|^{\,2}+\epsilon^2}\;, \tag{5}$$

where ϵ^2 is a positive small number, $W(x\,,\,z\,,\,t)$ is a weighting function depending on both the geometric spreading of wave propagation and the reliability of computed wavefields, and the sign function $\mathbf{sign}(x)$ equals $+1$ if $x > 0$, -1 if $x < 0$, and 0 if $x = 0$. Estimation of reflectivity using equations (2)-(5) is simply a zero-lag cross-correlation of the forward-modeled wavefield and the backward-extrapolated wavefield with a certain weighting function. Experiments have shown that estimation using equation (3) gives the best result with the least effort.

Synthetic results

Figure 3a shows a synthetic shot profile before migration. The profile contains reflections from two flat reflectors. The two flat reflectors are well imaged in Figure 3b by LITWEQ prestack migration. For flat-bed reflections, images will be obtained only on the near-offset side of the profile, since the profile only records reflections from this half of the section. Data-truncation effects caused by limited offsets are likely to be seen on both sides of the imaged reflectors (Figure 3b). Data extrapolation (Claerbout, 1985) on both sides of unmigrated profiles should suppress these truncation artifacts.

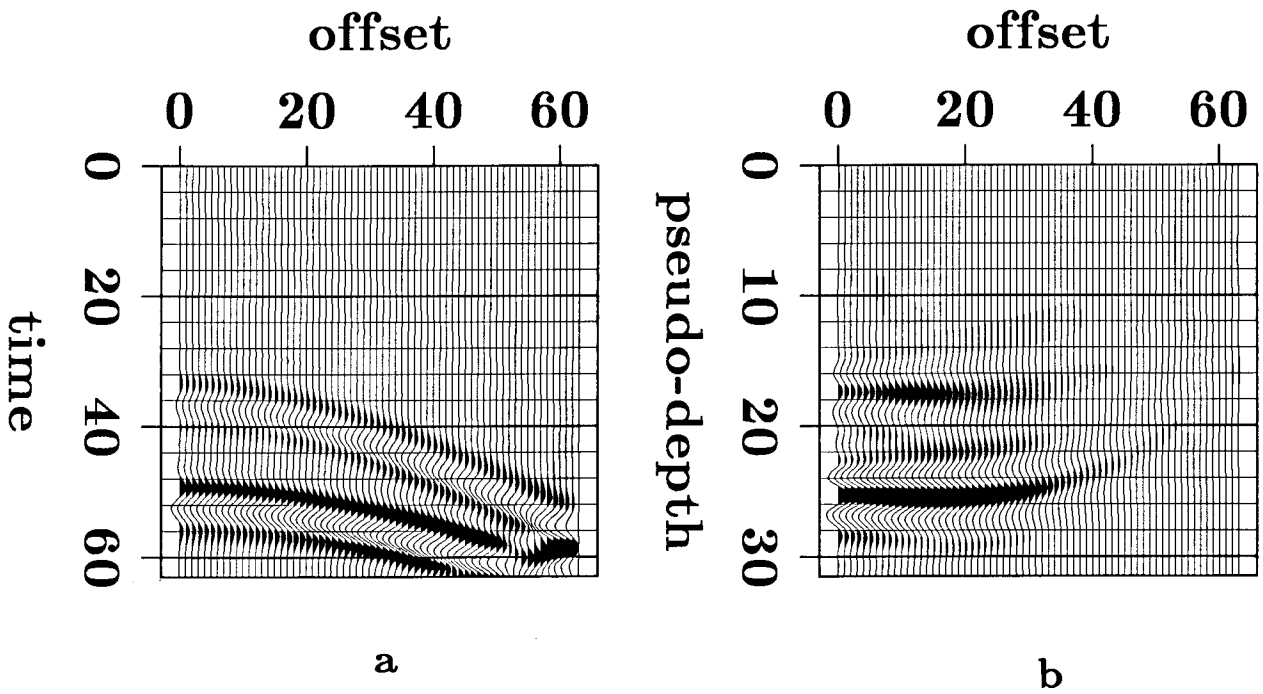

FIG. 3. **a.** Synthetic shot profile of reflections from a three-layer model. Thicknesses of the three layers are $\Delta\tau_1 = 17$, $\Delta\tau_2 = 7$ and $\Delta\tau_3 = \infty$. Velocities are $v_1 = 1.5$, $v_2 = 2$ and $v_3 = 3$. **b.** Migrated profile of the three-layer model.

Figure 4 shows a profile migration of dipping reflections generated from a 45-degree fault plane. After migration, a τ-z conversion is made to obtain the migrated depth section shown in Figure 4b. The fault plane is imaged as the result of this prestack migration process (Figure 4).

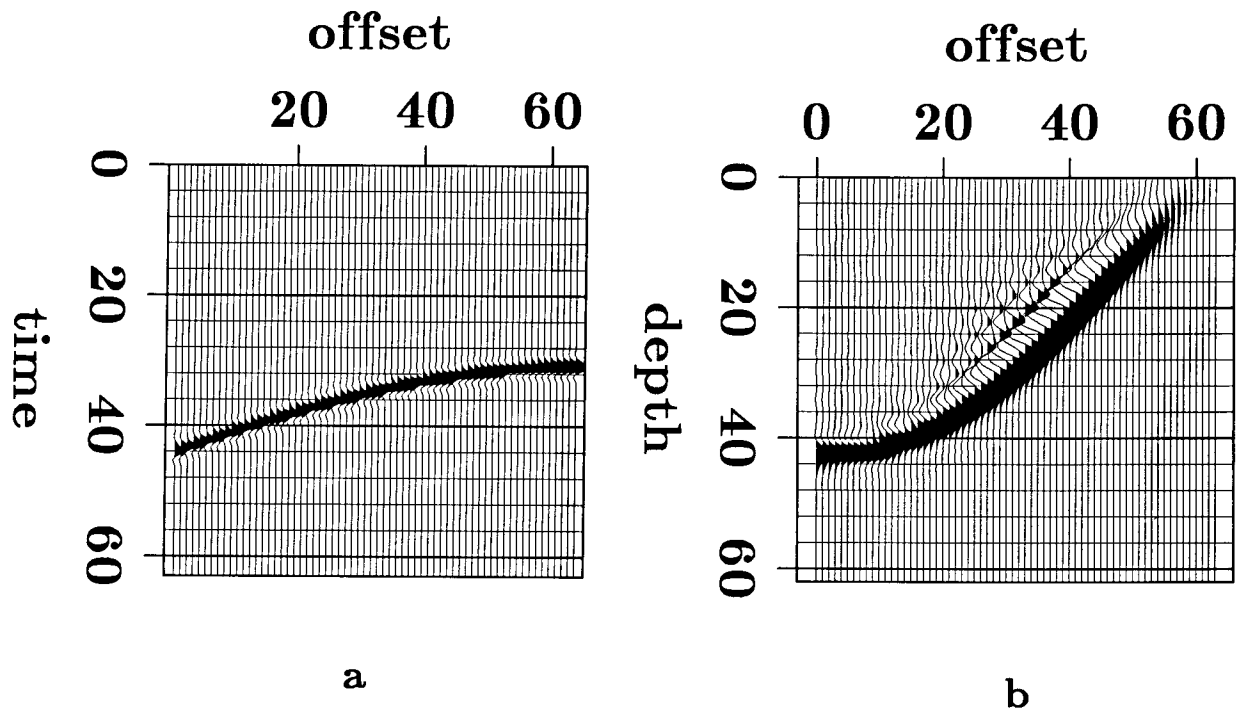

FIG. 4. **a.** Synthetic shot profile of reflections from a 45-degree dipping-fault plane model. The velocity above the fault plane is $v_1 = 2$, while the velocity below is $v_2 = 3$. **b.** Migrated depth section of the fault plane. Data truncation effects can be seen at both sides of the imaged fault plane.

Field data results

LITWEQ prestack migration was applied to 56 shot gathers from the Gulf of Mexico. The profiles contain both flat-bed and dipping fault-plane reflections. Figure 5a shows one of the shot gathers. We will pay special attention to a fault-plane reflection appearing at about 1.4 seconds on the nearest offset and at 1.3 seconds on the farthest offset (marked by **D** in Figures 5a and 5b), and to multiple reflections appearing below the primary reflection (marked by **F**) at 2.25 seconds on the nearest offset and 2.5

seconds on the farthest offset.

Figure 6 shows the migrated version of the profile of Figure 5a. Flat reflectors are all imaged well in the migrated section. Notice that the dipping fault plane is also nicely imaged with high resolution and that the multiple reflections after the imaged flat reflector (at 1.1 seconds in pseudo-depth) are suppressed in the final section. Some tilted events in the right-hand side of the final section are reflections from sides of computational grids. These boundary reflections are incoherent and hence will be reduced when we finally stack different migrated profiles, though absorbing boundary conditions should be able to suppress them.

STACKING OF MIGRATED PROFILES

Each migrated profile provides a picture of a certain portion of the underground structures, and these pictures usually overlap with adjacent ones. The images in different migrated profiles will be coherent, or aligned, if the correct velocity function is used in the migration of all profiles. Stacking of these coherent images certainly enhances the resolution of the underground structures, while suppressing incoherent noises (reverberations and boundary reflections). Stacking uses the following formula

$$\textbf{Image}(x\,,\,z) \;=\; \sum_{is=1}^{NS} \frac{C_{is}(x\,,\,z)}{N(x)}\,, \tag{6}$$

where NS is the number of shots in a survey line, and $N(x)$ is the number of ray coverages in position x.

Five of the 56 migrated profiles mentioned in the last section have been chosen and displayed in Figure 7. The images of these migrated profiles are aligned exactly. Stacking over these 56 separated images offers a clearer picture of underground structures (Figure 8) than that provided by any individual migrated profile. Notice again that in Figure 8 the dipping fault plane is well imaged, while the computational boundary reflections we saw in Figure 5 are suppressed.

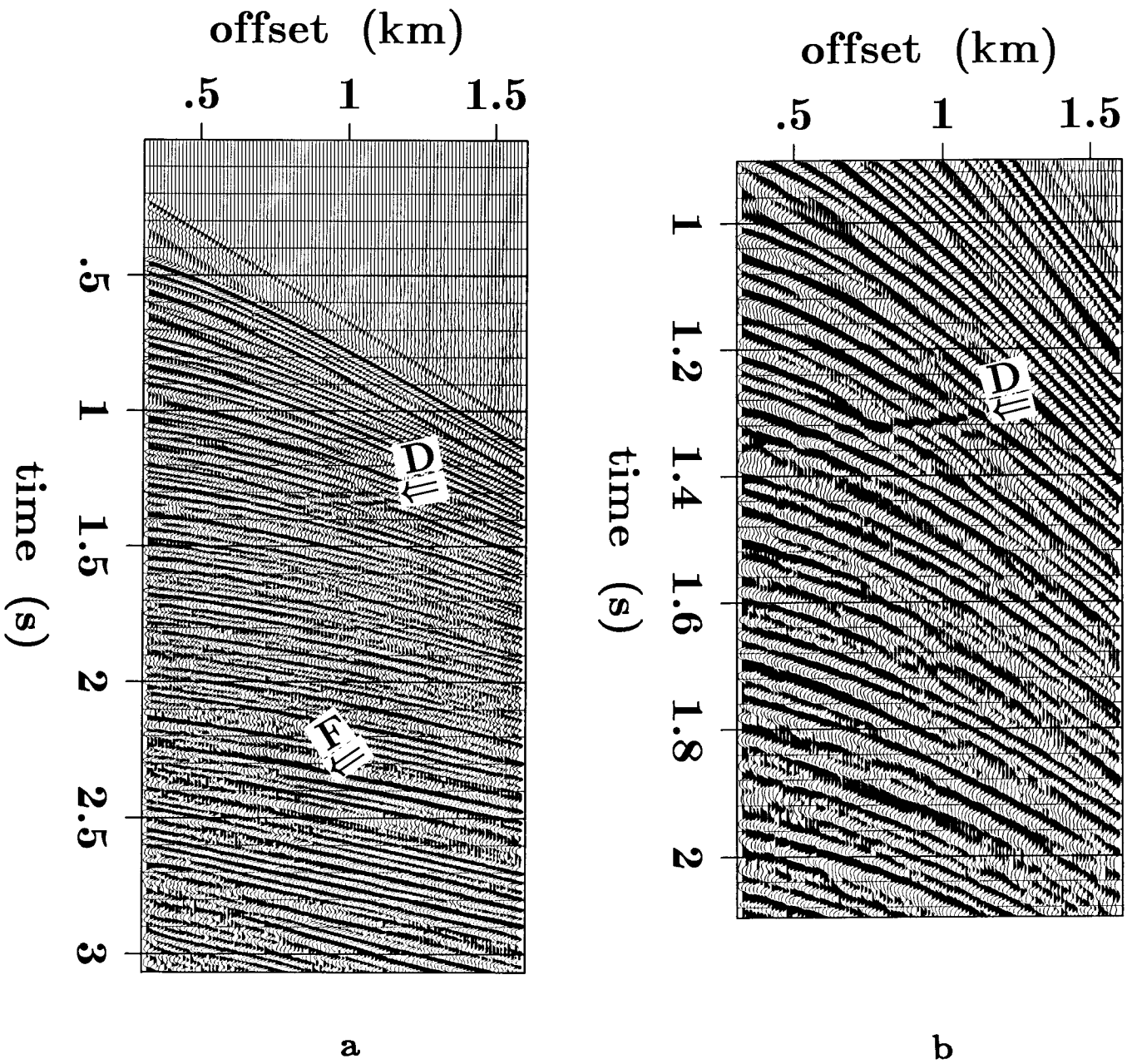

FIG. 5. **a.** A shot gather from the Gulf of Mexico. Reflections from a dipping fault plane can be seen at about 1.4 seconds at the nearest offset and at 1.3 seconds at the farthest offset, as marked by **D.** Some multiple reflections after a strong flat-bed reflection (marked by **F**) at bout 2.25 seconds at the nearest offset and at 2.5 seconds at the farthest offset are present in the gather. **b.** Amplified display of a window of profile in Figure 5a. The reflection from a fault plane (dipping to the left) can be seen clearly in the figure.

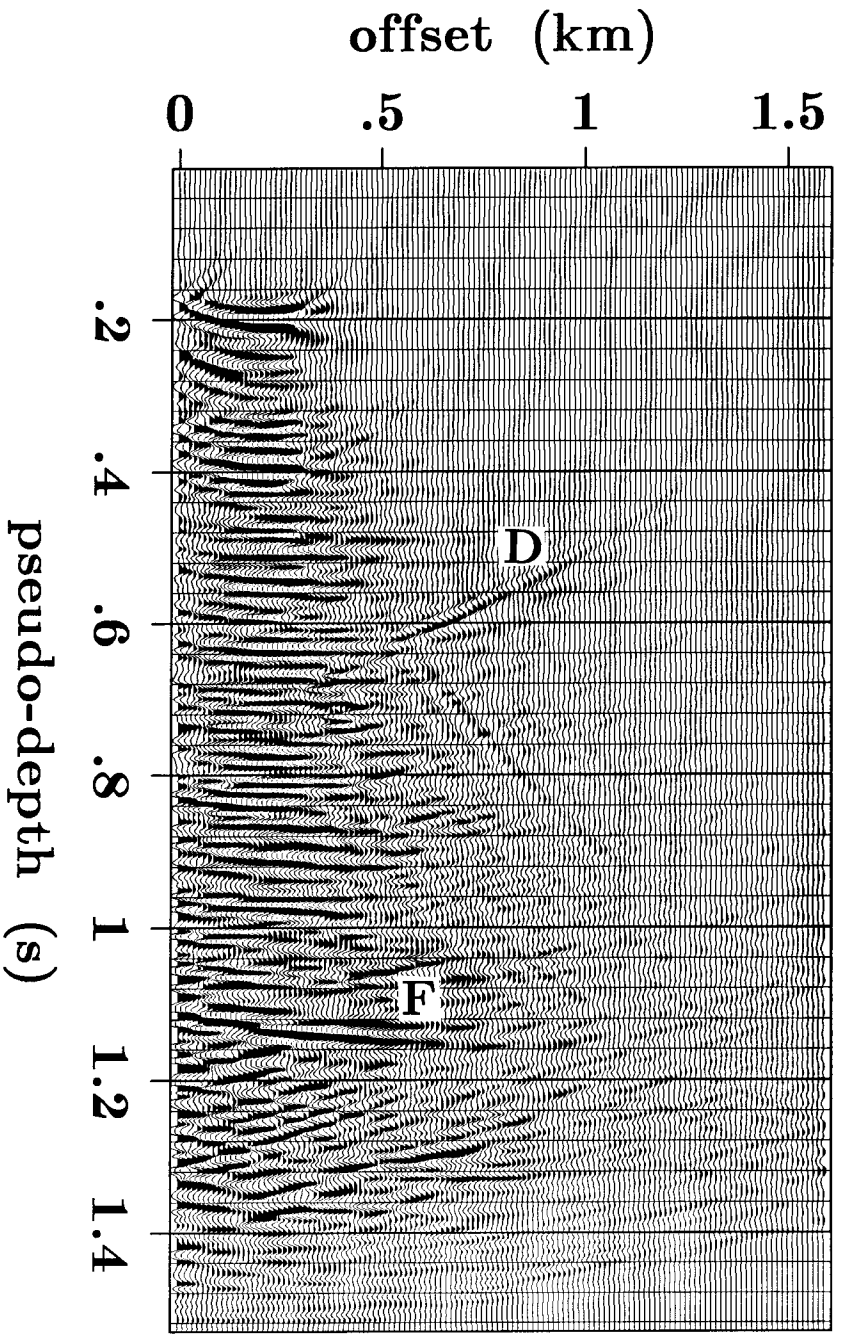

FIG. 6. Migrated profile of the gather in Figure 5. The dipping fault plane is well imaged. The multiple reflections existed in Figure 5.a have been suppressed in the migrated profile, while the flat-bed reflection above them is migrated to about 1.1 seconds of pseudo-depth.

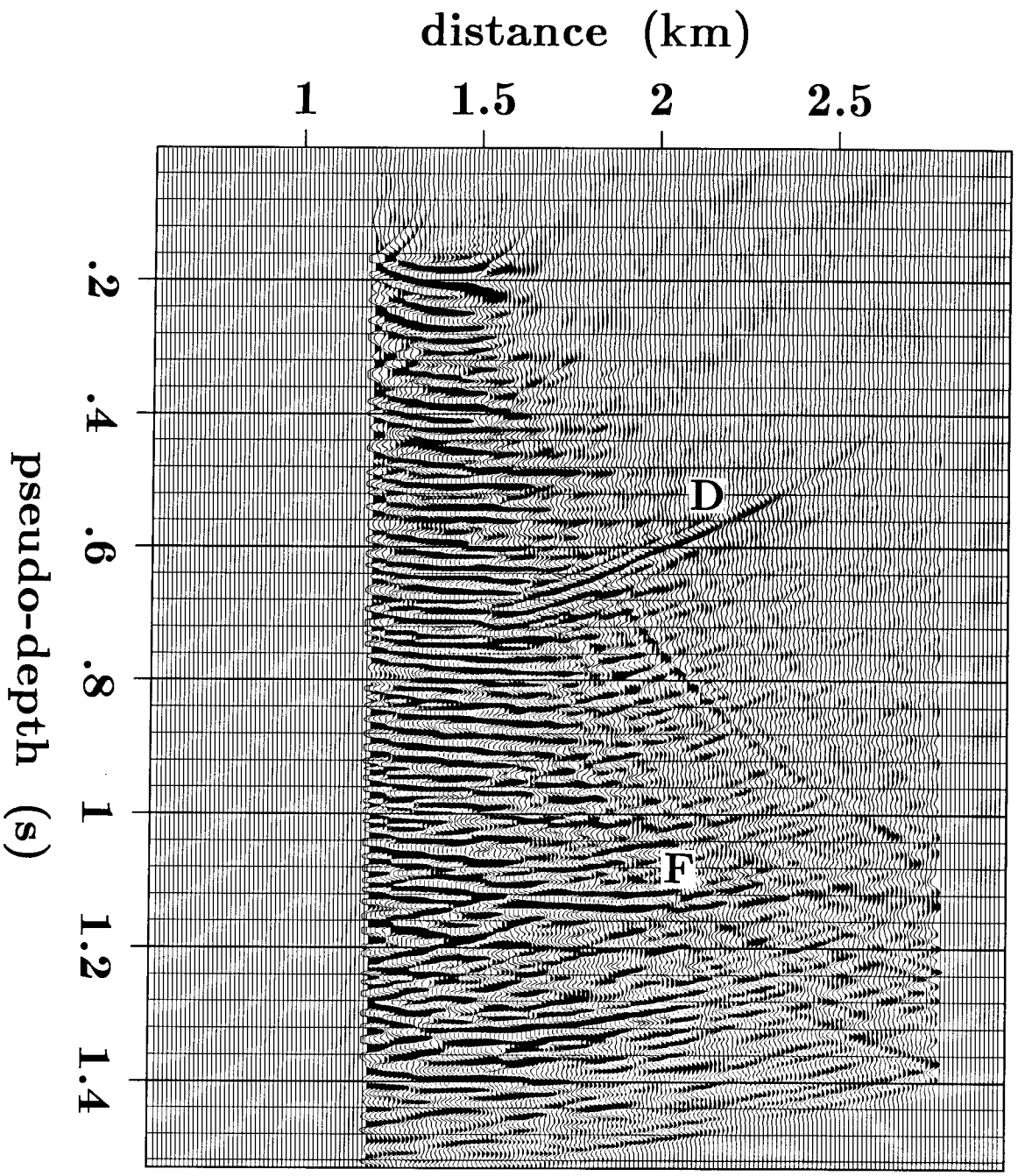

FIG. 7a. Migrated profile of shot gather s8.

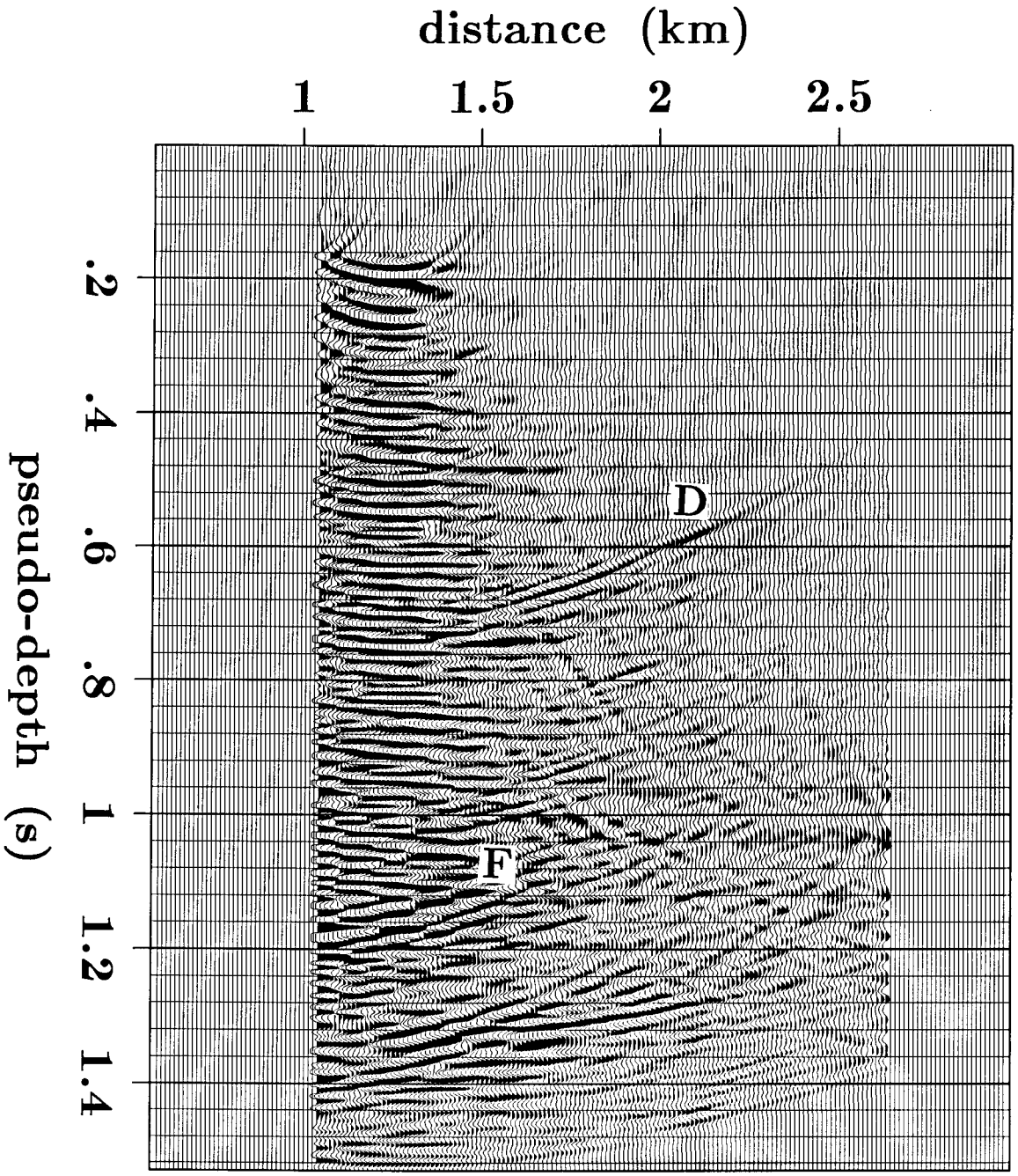

FIG. 7b. Migrated profile of shot gather s14.

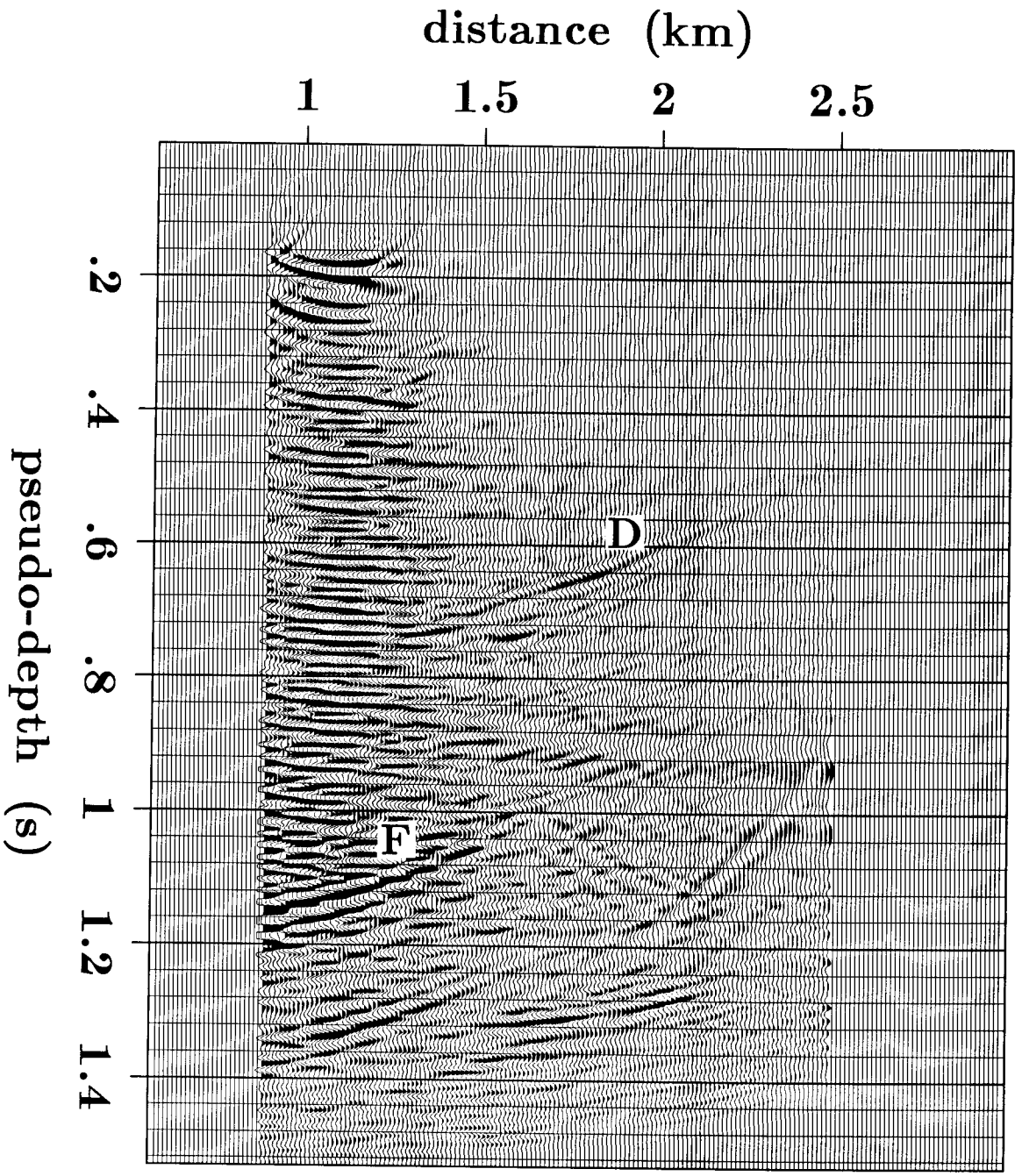

FIG. 7c. Migrated profile of shot gather s20.

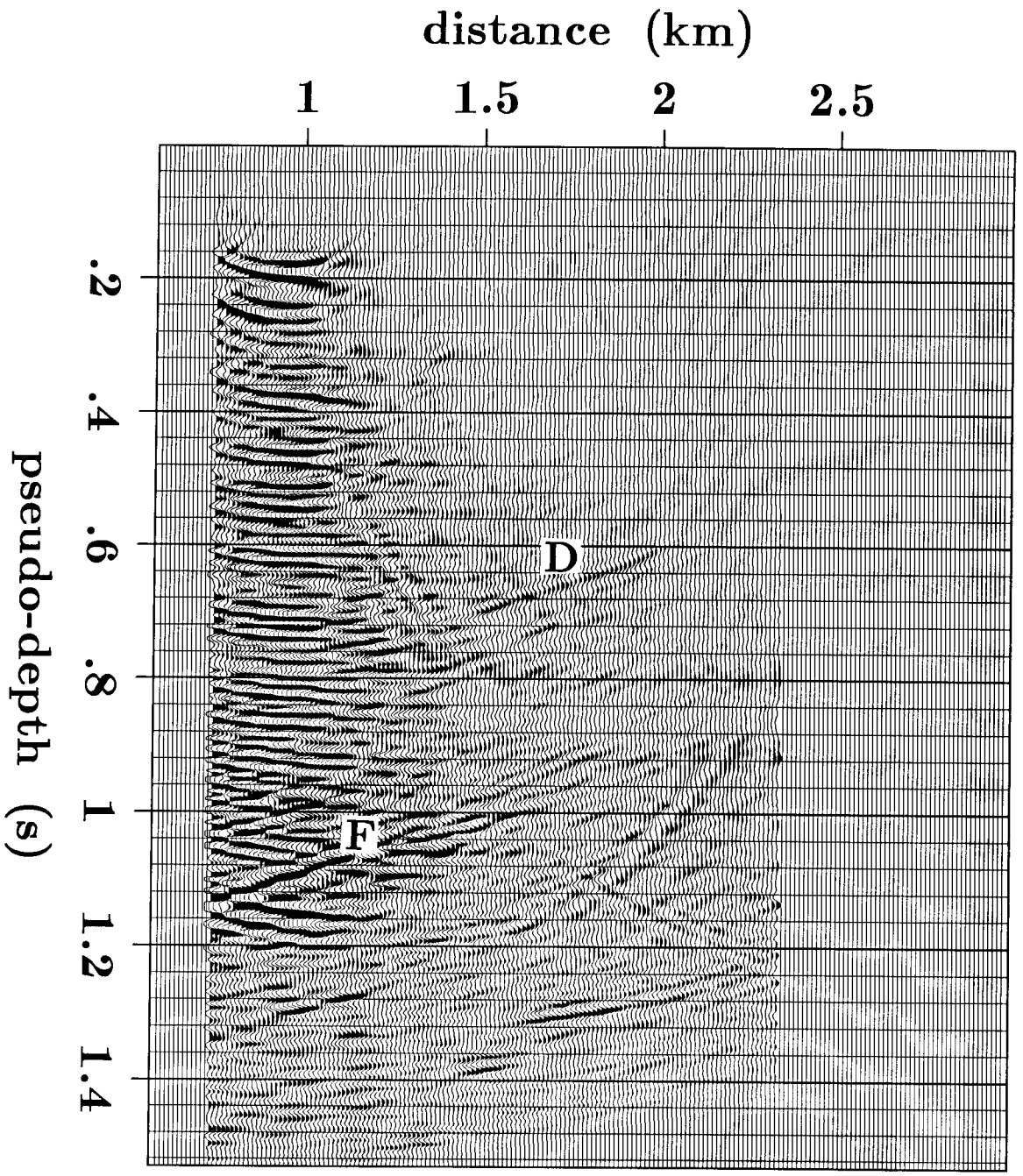

FIG. 7d. Migrated profile of shot gather s26.

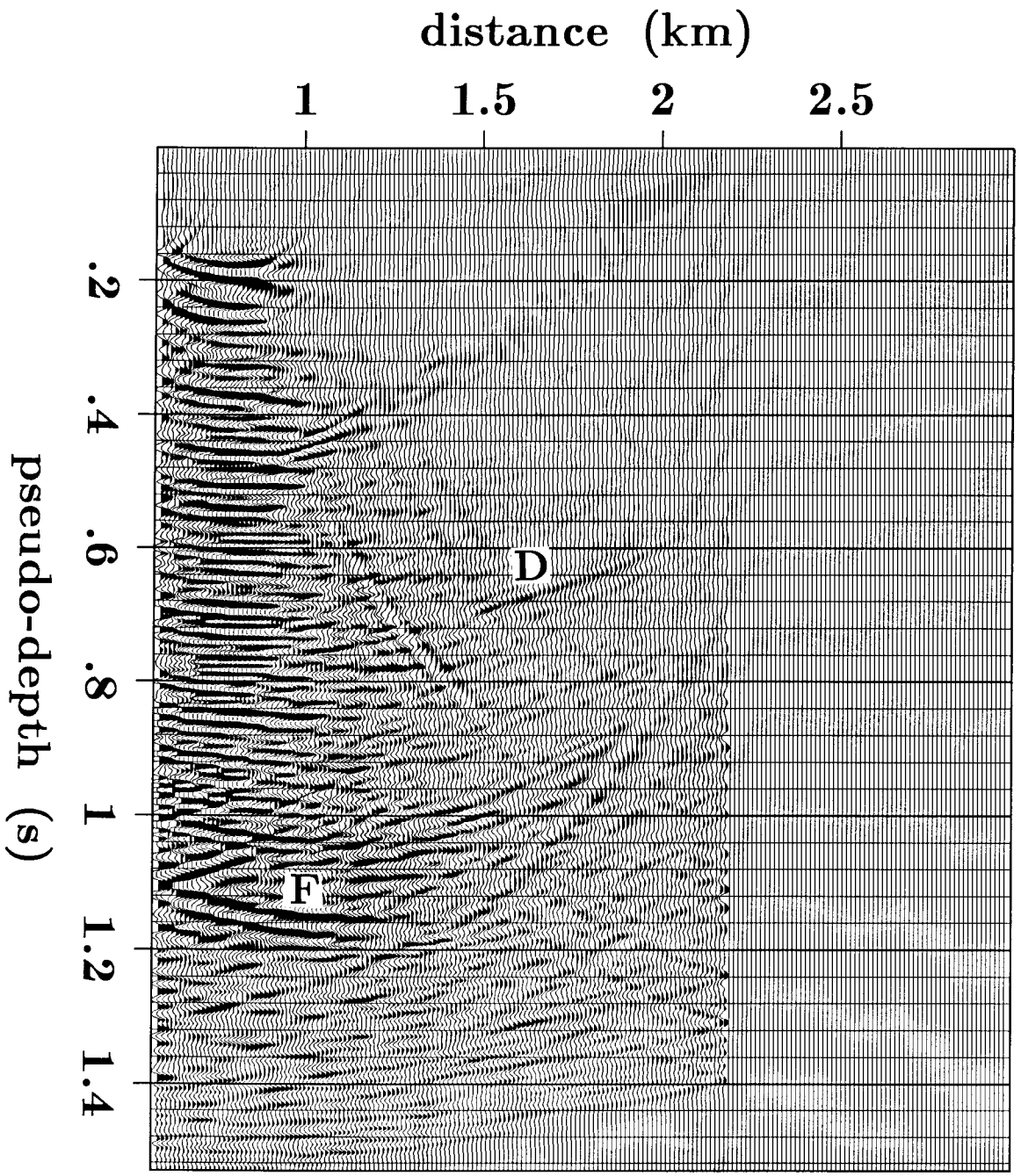

FIG. 7e. Migrated profile of shot gather s32.

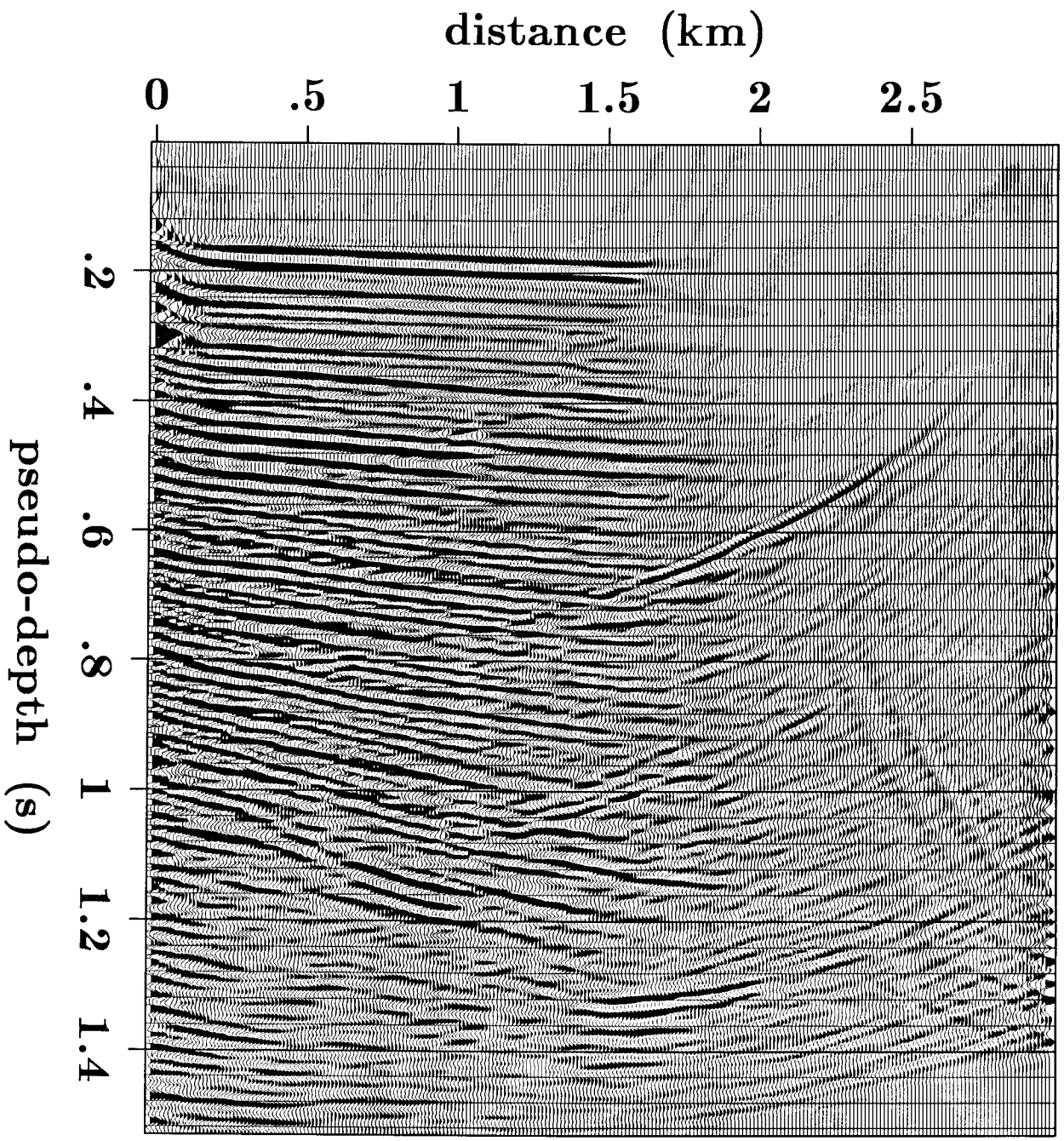

FIG. 8. Stacked section of migrated profiles. Boundary reflections and some incoherent noises are suppressed, while reflector images are enhanced. The fault plane is imaged with high resolution.

FUTURE WORKS

Velocity analysis by maximizing stacking power

Stacking migrated profiles over shot axis s using equation (5.6) yields the maximum power when the velocities used in the migrations are correct. Therefore, scanning through a range of velocities and maximizing the stacked power at a certain depth provides a method for picking the correct velocity at that depth. The same procedure will then be carried out to estimate velocities for the next depth of interest by downward extrapolating later arrivals through shallower depths using the known velocities estimated earlier and scanning through certain ranges of velocities for the deeper part of the section, until all velocities from the surface to the maximum depth of interest are obtained.

Under the assumption of local lateral homogeneity and flat layered medium (as in conventional velocity analysis from CMP gathers), velocity analysis of common-shot gathers is as simple as conventional velocity analysis of CMP gathers, since similar normal-moveout-correction formulas can be used, and we do not need to migrate and then stack to estimate velocity. However, this approach will give root-mean-square (RMS) velocities of the earth instead of the interval velocities that can be obtained using the method of migration and stacking.

When velocity varies laterally, the method of migration and stacking should be used, though it is possible to apply a moveout correction by ray tracing. There may be two approaches in the method of migration and stacking to invert velocity. The first one is to do constant-velocity migrations of all profiles and stacking, in a similar way to Toldi's scheme (Toldi, 1985) or Fowler's scheme (Fowler, 1984). The second one is to invert velocity by perturbing velocity model and iterating profile migrations.

Imaging multiple reflections and other types of waves

As discussed in the preceding sections, LITWEQ profile migration images underground structures by cross-correlating downward-continued primaries and downgoing incident waves, while suppressing incoherent noises such as multiple reflections. If computations of both the forward modeling and the backward extrapolation are done over the whole rectangular region $0 \leq t \leq t_{\max}$ and $0 \leq s \leq s_{\max}$, as happens in two-way LITWEQ modeling, then not only primary reflections but also multiple reflections may be migrated to the proper reflector positions and become coherent.

CONCLUSION

The LITWEQ wavefield extrapolation method can be applied to prestack migration of seismic data. Further applications of the LITWEQ profile migration method may be in seismic inversion and multiples extrapolation.

ACKNOWLEDGMENTS

I thank Bill Harlan and Stew Levin for their helpful suggestions and discussions in this work. Thanks are also due to Chevron for supplying the field dataset.

REFERENCES

Claerbout, J. F., 1976, Fundamentals of geophysical data processing: McGraw-Hill.

Claerbout, J. F., 1985, Imaging the earth's interior: Blackwell Scientific Publications.

Fowler, P., 1984, Incorporating dip corrections in velocity analysis anomalies: SEP-38, 113-132.

Hale D., 1983, Dip-moveout by Fourier transform: Ph.D. thesis, Geophysics Department, Stanford.

Jacobs A., 1982, The pre-stack migration of profiles: Ph.D. thesis, Geophysics Department, Stanford.

Judson, D.R., Schultz, P.S., and Sherwood, J.W.C., 1978, Equalizing the stacking velocities of dipping events via Devilish: Presented at the 48th Annual International SEG Meeting in San Francisco.

Li, Z., 1985, Wave field extrapolation by the linearly transformed wave equation operator: SEP-41, 167-189.

Li, Z., 1985, Linearly transformed wave equation modeling: SEP-42, 363-372.

Mayne, W.H., 1962, Common reflection point horizontal data stacking techniques: Geophysics, **27,** 927-938.

Toldi J., 1985, Velocity Analysis without picking: Ph.D. thesis, SEP-43, Geophysics Department, Stanford.

Student Work Hours --- Work "peaks" occur at noon, 4PM, and 10PM.

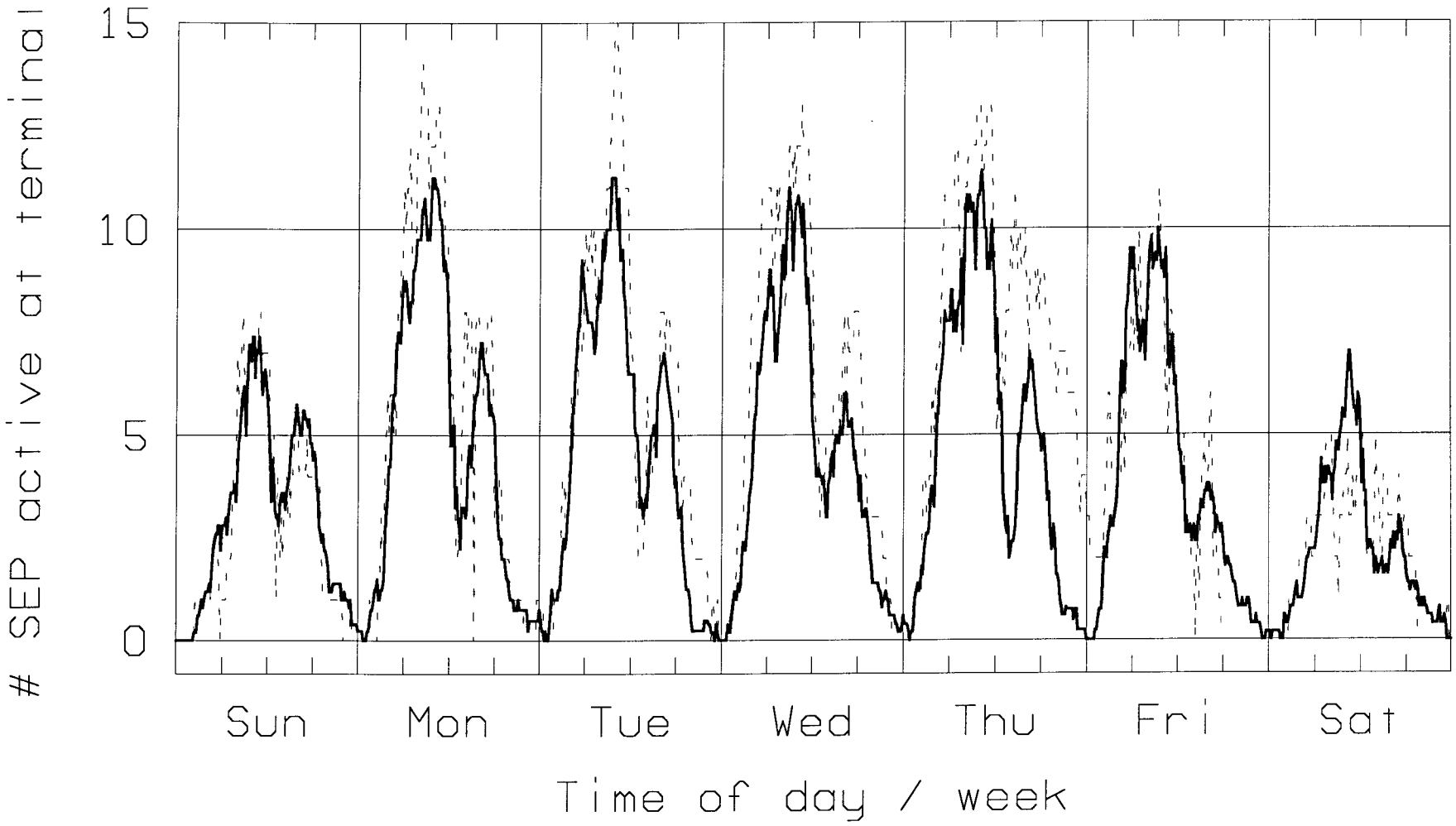

A graph showing how many SEP people are working on the system as a function of time of week. "Working" means logged in and having typed something within the last hour. Care is taken not to count the same person twice. The maximum count possible is 16, although this was never achieved. The dark curve shows the average over the last 2 months excluding the week right before report deadline; the thin dotted curve shows this final week. Deadline (as should be clear from the chart) was Friday morning. Days are considered to begin at 6AM.